Gauging error of pose acquired by vision systems in bin picking applications

Marek Franaszek*, *Prem* Rachakonda, and *Kamel S.* Saidi

National Institute of Standards and Technology, 100 Bureau Drive, Gaithersburg, MD 20899-8230, USA

Abstract. Picking a part from an unorganized pile of parts requires an accurate vision system integrated with a robotic arm. A proper metric for gauging pose error is therefore indispensable. Pose error is a combination of an error in the position vector and an error in the orientation matrix. Pose errors of a system under test (SUT) are calculated by comparing the poses obtained with the SUT with those obtained using a ground truth (GT) system whose measurements are registered to the SUT coordinate frame. Typically, the position error is calculated as the length of a vector connecting the SUT and the registered GT positions, and the orientation error is determined as the angle of relative rotation between the SUT and the registered GT orientation. However, many parts processed in industrial bin picking applications have axial symmetry and for such parts, the orientation cannot be determined uniquely. This causes the common metric for orientation error to be ambiguous and misleading. We show that a better and more reliable orientation metric can be calculated as the angle between the axes of symmetry for a part in the SUT and in the registered GT coordinate frame.

1 Introduction

Bin picking is a frequently deployed solution in manufacturing to automate tasks such as assembly or kitting. Its goal is to autonomously pick up a single part from an unorganized pile of parts and pass it to the next stage of the automated process. Successful completion of this goal requires a well calibrated robot integrated with the vision system, which must provide to the robot controller with the pose of each part. A part's pose (i.e., its position and orientation) needs to be accurately determined, to a degree related with a part's size, so that a gripper can approach and grab the part. Of the performance metrics that can be used to determine the suitability of a vision system for a particular application, pose error is a prominent one [1, 2].

However, pose error is usually not provided in the system's specification and there are few, non-trivial reasons for it. First, a six degree of freedom (6DoF) pose is rarely directly measured. Typically, raw data acquired either from 2D images or 3D point clouds are processed using various algorithms which output the 6DoF poses of parts [3, 4]. This means that the same data processed by different algorithms or different quality data input to the same algorithm may yield different results. Second, pose measuring systems provide their output in their own coordinate frames. Thus, the pose measured with the system under test (SUT) cannot be directly compared with that provided by a ground truth (GT) system. To calculate error in the SUT pose, the GT data must first be registered to the SUT frame and the registration error propagates into SUT pose error. Third, some objects may have axial symmetry and multiple equivalent orientations. Therefore, the standard way of gauging orientational misalignment as the angle of relative rotation between the SUT and the GT poses may be ambiguous and such objects are quite common in manufacturing applications.

In this paper, we specifically describe a novel method of gauging pose error of parts with axial symmetry that are randomly piled in a bin. We show that a better metric for such parts requires first fitting the computer-aided-design (CAD) model of the part to the SUT and GT point cloud data, and then reporting orientation error as the angle between the axes of symmetry of the two fitted CAD models. Attempts to derive pose errors directly from the 3D points acquired by the SUT and the GT sensors often yields ambiguous and incorrect results.

2 Previous work

For systems that determine pose from a set of markers, the influence of noise and bias in the marker locations on the derived pose was extensively studied [5, 6] and the standard for evaluating the performance of such systems was adopted [7]. For other systems, which do not rely on markers but derive pose from 3D point clouds, some bounds on pose variation may be obtained if the bounds of the noise affecting the 3D points are known [8], but such methods fail for objects with symmetry. The development of standards for 3D imaging system performance for use in automating the manufacturing process are an ongoing effort [9].

Symmetry of parts was specifically addressed in Maximum Symmetry-Aware Surface Distance (MSSD) used in benchmarking the 6D Object Estimation (BOP) challenge [10]. This metric has unit of length (e.g., mm)

* Corresponding author: marek@nist.gov

and requires prior determination of the symmetries that characterize a given part [11-13]. The MSSD metric is also used in a recently initiated perception challenge for bin picking [14].

3 Apparatus and test setup

In this work, two different systems were used to obtain the 3D data. The first one was a structured light camera mounted in a fixed position, the SUT. The second one was a laser line probe mounted on an Articulating Arm Coordinate Measuring Machine (AACMM), used as a GT system. The GT system acquires the data from various directions and automatically registers data. The SUT outputs data in the format of an organized 3D point cloud $\boldsymbol{s}_i$ of size $(N_{row}, N_{col}, 3)$, derived from the depth images of size (N_{row}, N_{col}), such as shown in **Fig. 1**. The GT system outputs an unorganized 3D point cloud $\boldsymbol{g}_j$. Both systems acquire the 3D point clouds in their respective coordinate frames.

Fig. 1. Example of a depth image acquired with the SUT.

Two different kinds of symmetric parts were used: M8 socket head cap screws and M12 hex nuts, both made from the same material. A bin was randomly filled with one kind of parts and scanned with both systems. This step was repeated for $K = 3$ different instances of random piles in the bin and for both kinds of parts.

4 Data processing

The data from the SUT were processed using the Segment Anything Model (SAM) algorithm [15]. SAM was applied to the depth images acquired by the SUT to automatically segment individual parts in the 2D Depth image of the bin. Once the resulting binary 2D masks of parts were obtained for each k-th instance of a pile in the bin ($k \leq K$), $M = 20$ masks were randomly selected, and their corresponding subsets of 3D points $\boldsymbol{S}_{m,k}$ were obtained, $m = 1, \dots, M$ (see **Fig. 2**). This procedure was repeated for both the M8 screws and M12 nuts.

4.1 Registering GT to SUT frame

For each k-th instance of a pile of parts in a bin acquired by the SUT and the GT, the top part of a bin was manually segmented. The Iterative Closest Point (ICP) procedure was then used to get the rigid body transformation, $\boldsymbol{T}_k$, which can be used to register the GT frame to the SUT frame [16]. The outcome of this procedure is shown in **Fig. 3**. As the exit condition from ICP, the maximum number of iterations $I_{max} = 10$ was used.

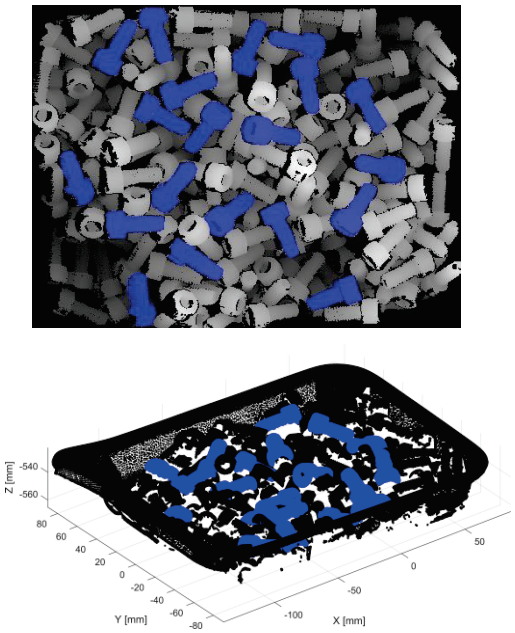

Fig. 2. Example of segmentation masks generated automatically by SAM applied to 2D depth image (upper plot) and the corresponding 3D point cloud (lower graph). Segmented parts colored in blue.

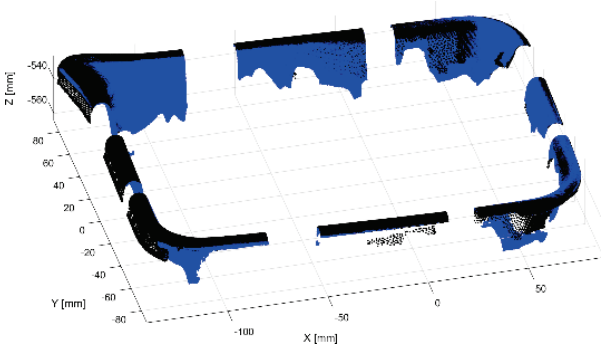

Fig. 3. Example of registering segmented bin from GT frame (black points) to SUT frame (blue points). For better visualization, portions of data are not displayed.

Once $\boldsymbol{T}_k$ was determined for each k-th instance of a pile, the GT data were transformed to the SUT coordinate frame. Then, for each selected earlier subset, $\boldsymbol{S}_{m,k}$ in the SUT data, the corresponding subset of 3D points, $\boldsymbol{G}_{m,k}$ from the transformed GT data was manually segmented.

4.2 Getting pose error without CAD fitting

For each k-th pile instance and each selected m-th part, the subset of 3D points, $\boldsymbol{G}_i$ was registered to $\boldsymbol{S}_i$ using ICP (to simplify notation, the part index i is used, $i = 1, \dots, M \times K$). The outcome of this procedure is shown in **Fig. 4**. Initial pose for ICP was selected as in [17].

This step resulted in the individual transformations $\boldsymbol{T}_i = (\boldsymbol{R}_i, \boldsymbol{t}_i)$, where $\boldsymbol{R}_i$ is the rotation matrix and $\boldsymbol{t}_i$ is the translation vector. In this case, the position error p_i is expressed as the length of the translation as

$$p_i = \|\boldsymbol{t}_i\|, \tag{1}$$

and the angle β_i of rotation $\boldsymbol{R}_i$ is used as the orientation error, where

$$\beta_i(\boldsymbol{R}_i) = arcos((tr(\boldsymbol{R}_i) - 1)/2) \tag{2}$$

and $tr(\boldsymbol{R})$ is the trace of a matrix $\boldsymbol{R}$.

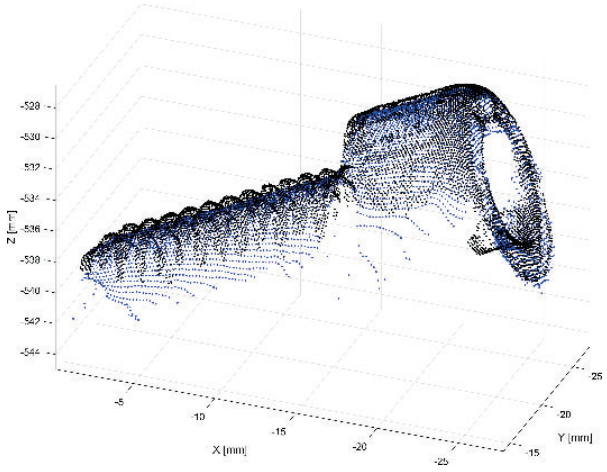

Fig. 4. Example of registering segmented 3D points $\boldsymbol{G}_i$ acquired by GT (black dots) to segmented $\boldsymbol{S}_i$ points (blue) acquired by SUT.

4.3 Calculating pose error using CAD fitting

Appropriate CAD models were also fitted to $\boldsymbol{S}_i$ and $\boldsymbol{G}_i$ using ICP for each i (i.e., each k-th pile instance and each selected m-th part), as shown in **Fig. 5**. This procedure yielded orientation matrices $\boldsymbol{\Omega}_{S,i}$ and $\boldsymbol{\Omega}_{G,i}$, and translation vectors $\boldsymbol{\tau}_{S,i}$ and $\boldsymbol{\tau}_{G,i}$. Based on these quantities, the orientation error $\omega_i(\boldsymbol{\Omega}_i)$, calculated as in (2), was determined as the angle of rotation of the relative rotation matrix $\boldsymbol{\Omega}_i$ as

$$\boldsymbol{\Omega}_i = \boldsymbol{\Omega}_{S,i}\, \boldsymbol{\Omega}_{G,i}^{-1} \tag{3}$$

where $\boldsymbol{\Omega}^{-1}$ is the inverse of matrix $\boldsymbol{\Omega}$. Position error e_i was then calculated as

$$e_i = \|\boldsymbol{\tau}_{S,i} - \boldsymbol{\tau}_{G,i}\|. \tag{4}$$

In addition, another orientation error α_i was calculated as the angle between the axes of symmetry $\boldsymbol{u}_{S,i}$ and $\boldsymbol{u}_{G,i}$ as

$$\alpha_i = arcos(\boldsymbol{u}_{S,i} \cdot \boldsymbol{u}_{G,i}) \tag{5}$$

where $\|\boldsymbol{u}_{S,i}\| = \|\boldsymbol{u}_{G,i}\| = 1$ and "·" is the dot product. Vector $\boldsymbol{u}_{S,i}$ was aligned with the axis of symmetry of a CAD model fitted to $\boldsymbol{S}_i$ and $\boldsymbol{u}_{G,i}$ was aligned with the axis of symmetry of a CAD model fitted to $\boldsymbol{G}_i$, as shown in **Fig. 6**.

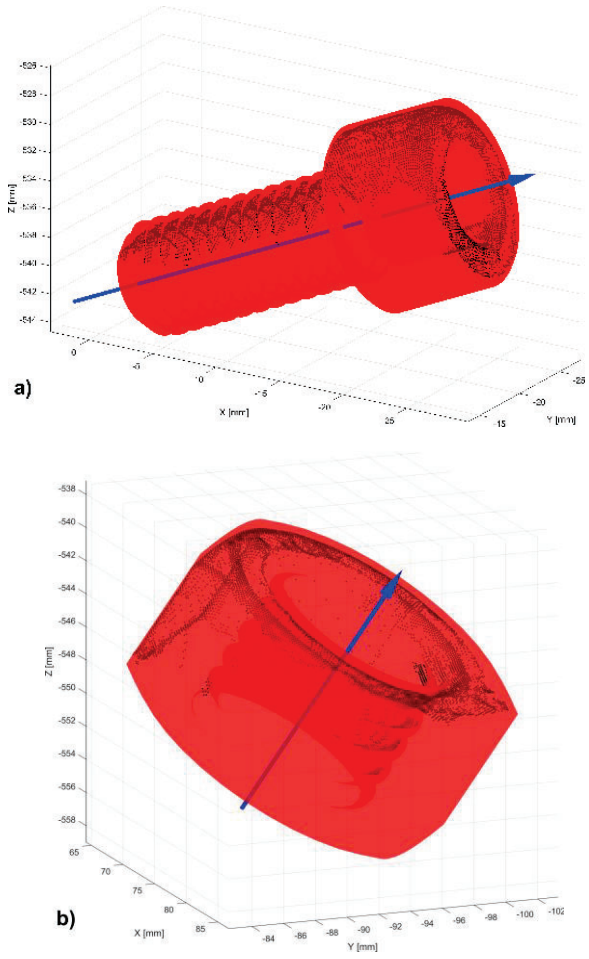

Fig. 5. Examples of CAD (in red) fitted to segmented 3D points (black dots) which belong to a): $\boldsymbol{S}_i$ acquired by SUT; b) $\boldsymbol{G}_i$ acquired by GT and transformed to SUT frame. Blue arrows represent axes of symmetry determined from CAD models.

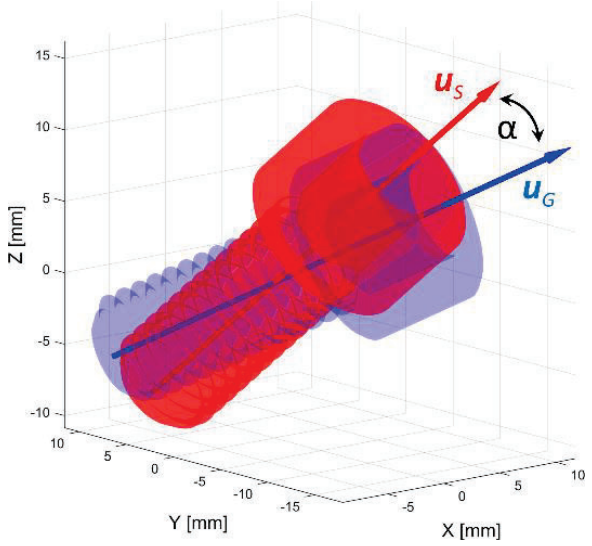

Fig. 6. Two CAD models fitted to $\boldsymbol{S}_i$ and the corresponding $\boldsymbol{G}_i$ subsets. Arrows represent the axes of symmetry, parallel to the unit vectors $\boldsymbol{u}_S$ and $\boldsymbol{u}_G$, the angle α is an acute angle between unit vectors.

5 Results

The outcome of the procedure described in Section 4.2. is presented in **Fig. 7** for a bin filled with M2 socket head cap screws. In this procedure, CAD models were not used and the pose error was calculated by registering the subset of 3D points $\boldsymbol{G}_i$ to $\boldsymbol{S}_i$ and by calculating the position error p_i from (1) and the orientation error β_i from (2). In addition, the residual ICP registration error e_{pc} is plotted in **Fig.** 7a and a distance Δ_i between two centroids $\overline{\boldsymbol{S}}_i$ and $\overline{\boldsymbol{G}}_i$ as

$$\Delta_i = \|\overline{\boldsymbol{S}}_i - \overline{\boldsymbol{G}}_i\| \,. \tag{6}$$

The corresponding results for a bin filled with M12 nuts are shown in **Fig. 8**.

The outcome of the procedure described in Section 4.3 is presented in **Fig. 9** for a bin filled with M8 screws. In this procedure, CAD models were fitted to each subset of 3D points $\boldsymbol{S}_i$ and $\boldsymbol{G}_i$, and the resulting two transformations $(\boldsymbol{\Omega}_{S,i}, \boldsymbol{\tau}_{S,i})$ and $(\boldsymbol{\Omega}_{G,i}, \boldsymbol{\tau}_{G,i})$ were used to characterize the error of the pose provided by the SUT. In **Fig. 9**a, the residual ICP error of fitting CAD to $\boldsymbol{G}_i$ is plotted. **Fig. 9**b shows distance e_i (calculated from (4)) between the positions of the fitted CAD models. In **Fig. 9**c, the rotation angle ω_i of a matrix of relative rotation $\boldsymbol{\Omega}_i$ determined from (3) is plotted. Finally, in **Fig. 9**d, the angle α_i (calculated from (5)) and illustrated in **Fig. 6**, is plotted.

The corresponding results for a bin filled with M12 nuts are shown in **Fig. 10**.

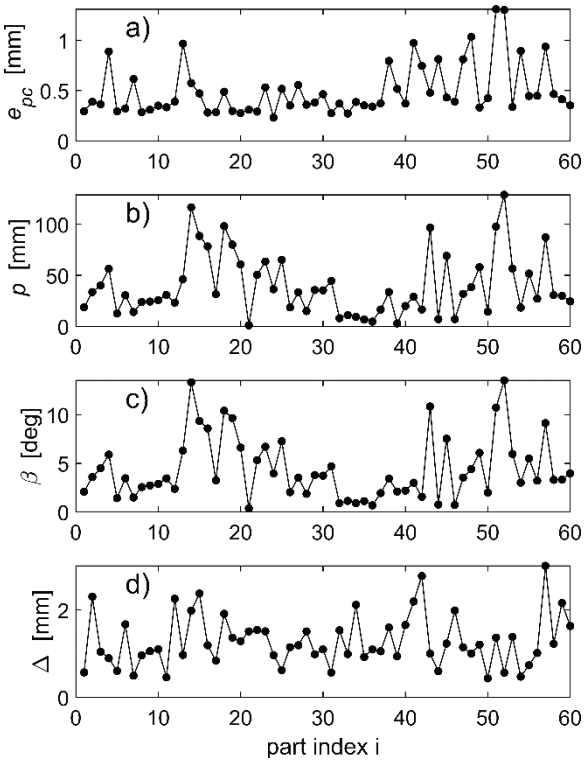

Fig. 7. Results for M8 screws: a) ICP error e_{pc} of registering point cloud $\boldsymbol{G}_i$ to $\boldsymbol{S}_i$; b) length p_i of the translation vector from ICP; c) rotation angle β_i from ICP; d) distance Δ_i between the centroids of $\boldsymbol{G}_i$ and $\boldsymbol{S}_i$.

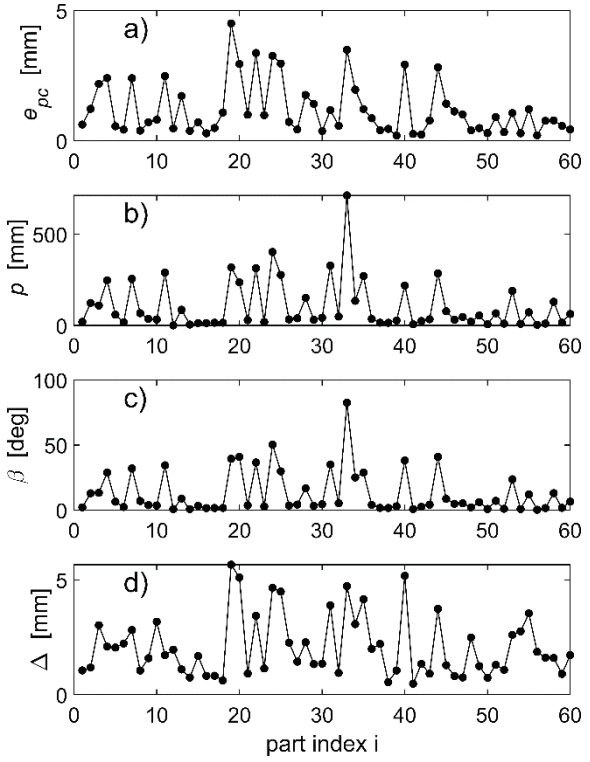

Fig. 8. Results for M12 nuts: a) ICP error e_{pc} of registering point cloud $\boldsymbol{G}_i$ to $\boldsymbol{S}_i$; b) length p_i of the translation vector from ICP; c) rotation angle β_i from ICP; d) distance Δ_i between the centroids of $\boldsymbol{G}_i$ and $\boldsymbol{S}_i$.

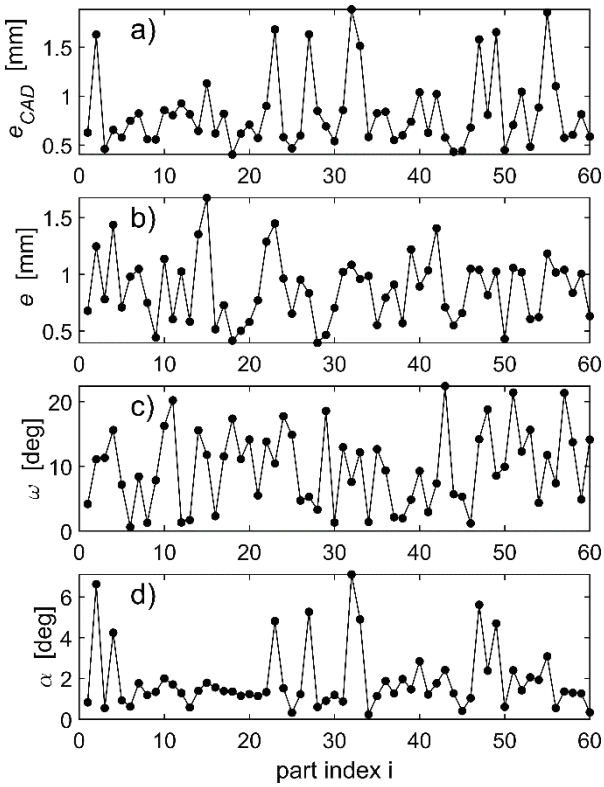

Fig. 9. Results for M8 screws: a) ICP error e_{CAD} of registering CAD to $\boldsymbol{G}_i$; b) distance e_i between the positions of CAD models fitted to $\boldsymbol{G}_i$ and $\boldsymbol{S}_i$; c) angle ω_i of relative rotation matrix $\boldsymbol{\Omega}_i$ in (3); d) angle α_i between axes of symmetry of CAD models fitted to $\boldsymbol{G}_i$ and $\boldsymbol{S}_i$.

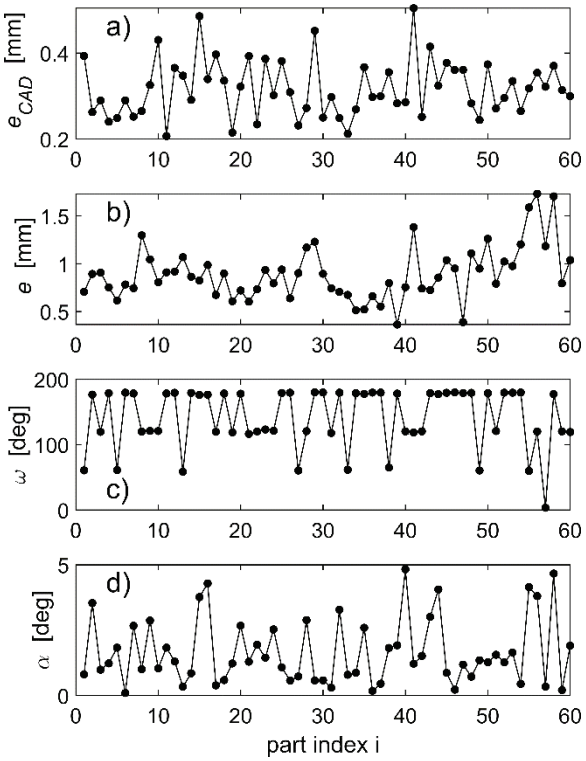

Fig. 10. Results for M12 nuts: a) ICP error e_{CAD} of registering CAD to $\boldsymbol{G}_i$; b) distance e_i between the positions of CAD models fitted to $\boldsymbol{G}_i$ and $\boldsymbol{S}_i$; c) angle ω_i of relative rotation matrix $\boldsymbol{\Omega}_i$ in (3); d) angle α_i between axes of symmetry of CAD models fitted to $\boldsymbol{G}_i$ and $\boldsymbol{S}_i$.

Table 1. Summary of mean errors

Mean Errors	**Screws M8**	**Nuts M12**
L_{min} [mm]	13.0	10.0
$\bar{e}_{pc}$ [mm]	0.50	1.11
$\bar{e}_{CAD}$ [mm]	0.83	0.32
$\bar{p}$ [mm]	39.43	96.69
$\bar{\Delta}$ [mm]	1.29	2.01
$\bar{e}$ [mm]	0.87	0.89
$\bar{\beta}$ [deg]	4.40	11.82
$\bar{\omega}$ [deg]	9.75	141.48
$\bar{\alpha}$ [deg]	1.88	1.65

6 Discussion

The ICP procedure was used in this study to register pairs of experimentally acquired, segmented subsets of points, such as shown in **Fig. 4**, or to fit CAD models to the experimental points, such as shown in **Fig. 5**. The rigid body transformations (rotations and translations) resulting from ICP were then used to evaluate different metrics, such as orientation errors β_i, α_i, ω_i and position errors p_i or e_i. Therefore, it is important to ensure that the poses obtained from the ICP procedure are correct, especially as the ICP process can be easily trapped in wrong local minima and can provide incorrect poses when an initial pose is not properly chosen.

All outcomes of ICP, such as displayed in **Fig. 4** and **Fig. 5**, were visually inspected, and the corresponding residual errors were checked. Examples of residual errors e_{pc} are plotted in **Fig. 7**a and **Fig. 8**a, and for e_{CAD} in **Fig. 9**a and **Fig. 10**a. Compared with the smallest size L_{min} of the bounding box containing the part, the registration was quite accurate as evidenced by small mean ICP errors $\bar{e}_{pc}$ and $\bar{e}_{CAD}$ in **Table 1**. Yet, the large values of some of the reported errors are in striking disagreement with visual evaluations and with the small values of the residual ICP errors.

Attempts to characterize pose error without fitting CAD models (as described in Section 4.2) yielded large orientation errors β_i displayed in **Fig. 7**c and **Fig. 8**c, see average errors $\bar{\beta}$ for screws and nuts in **Table 1**. The corresponding position errors p_i plotted in **Fig. 7**b and **Fig. 8**b seem to indicate a huge displacement between $\boldsymbol{S}_i$ and $\boldsymbol{G}_i$ 3D points (blue and black points in **Fig. 4**), which contradicts visual inspection and the displacements between centroids Δ_i plotted in **Fig. 7**d and **Fig. 8**d (compare also mean position errors $\bar{p}$ with mean displacements $\bar{\Delta}$ in **Table 1**).

It appears that incorrect displacement errors p_i, which are the length of the translation vectors $\boldsymbol{t}_i$ from ICP registration as in (1), are a consequence of ambiguous rotations $\boldsymbol{R}_i$ resulting from registering $\boldsymbol{G}_i$ to $\boldsymbol{S}_i$. In the ICP procedure, the translation vector $\boldsymbol{t}_i$ is obtained after the rotation matrix $\boldsymbol{R}_i$ is calculated as

$$\boldsymbol{t}_i = \overline{\boldsymbol{S}}_i - \boldsymbol{R}_i \overline{\boldsymbol{G}}_i \,, \tag{7}$$

where $\overline{\boldsymbol{S}}_i$ and $\overline{\boldsymbol{G}}_i$ are the corresponding centroids. If line-of-sight sensors are used to acquire 3D data (as is the case in many industrial bin picking applications) then the centroids $\overline{\boldsymbol{S}}_i$ and $\overline{\boldsymbol{G}}_i$ are not located on the part's axis of symmetry. Thus, the ambiguity of $\boldsymbol{R}_i$ in (7) must affect the vector $\boldsymbol{t}_i$ and this makes p_i an unsuitable metric for gauging position error (note the very strong correlation between p_i and β_i, displayed in **Fig. 7**b,c and **Fig. 8**b,c). Therefore, attempts to characterize the error of the pose based only on registration of the segmented 3D points $\boldsymbol{G}_i$ to $\boldsymbol{S}_i$ will be unsuccessful for parts with symmetry.

Deriving pose metrics from CAD models fitted to points $\boldsymbol{G}_i$ and $\boldsymbol{S}_i$, such as shown in **Fig. 5** and **Fig. 6**, is also challenging. While the position error e_i defined in (4) takes on reasonably small values in **Fig. 9**b and **Fig. 10**b (see mean errors $\bar{e}$ in **Table 1**), the orientation error ω_i, calculated from the matrix of relative rotation $\boldsymbol{\Omega}_i$ in (3) still has misleadingly large values ω_i plotted in **Fig. 9**c and **Fig. 10**c (see mean orientation errors $\bar{\omega}$ in **Table 1**).

It is worth noting that the ambiguity of the rotations $\boldsymbol{\Omega}_{S,i}$ and $\boldsymbol{\Omega}_{G,i}$ (from which $\boldsymbol{\Omega}_i$ is calculated) does not affect the translation vectors $\boldsymbol{\tau}_{S,i}$ and $\boldsymbol{\tau}_{G,i}$ (from which the position errors e_i are calculated) and, unlike position errors p_i which are flawed by large values, e_i provide appropriately small position errors. The root cause of the difference between p_i and e_i is that the centroids of the CAD models are located on the axes of symmetry and

therefore, ambiguities in rotations $\boldsymbol{\Omega}_{S,i}$ and $\boldsymbol{\Omega}_{G,i}$ around those axes do not affect translation vectors $\boldsymbol{\tau}_{S,i}$ and $\boldsymbol{\tau}_{G,i}$.

It appears that the angle α_i between the axes of symmetry, as illustrated in **Fig. 6**, provides a more realistic estimate of the orientation error, as shown in **Fig. 9**d, **Fig. 10**d and characterized by mean angles $\bar{\alpha}$ in **Table 1**.

For parts used in this study (M8 socket head cap screws and M12 hex nuts), the mean angle $\bar{\alpha}$ was sufficient to describe rotational misalignment, but generally, rotations around the axes of symmetry may also contribute to the overall error. In such cases, the total error will have a contribution from rotating $\boldsymbol{u}_G$ vector to $\boldsymbol{u}_S$, as in **Fig. 6**, and then an additional angular component resulting from a rotation around $\boldsymbol{u}_S$.

Using CAD models fitted to SUT and GT data and the mean angle $\bar{\alpha}$ as an orientation error may be more practical than MSSD in bin picking applications. To execute a successful pick, planning a gripper's approach to a part requires knowledge of the full CAD surface, including sections of the surface occluded during data collection. Therefore, the angular error of the CAD orientation may be more useful than the distance provided by MSSD, which is calculated only from points covering a fraction of the part's surface within line-of-sight of the sensor.

7 Conclusions

For parts with axial symmetry, the commonly used orientation error (defined as the angle of relative rotation between CAD models fitted to SUT and GT data) provides estimates which are unreliable and inconsistent with visual inspection. The angle between two axes of symmetry corresponding to two fitted CAD models are more useful in gauging the orientation error for such parts. Position error defined as the distance between the positions of two fitted CAD models also provides a useful metric.

Use of CAD models is crucial as the errors derived from registering two subsets of 3D points acquired by the SUT and the GT provide a misleading metric, which is inconsistent with visual inspection of the two datasets.

References

[1] H. Alzarok, S. Fletcher, and A. P. Longstaff, "Survey of the current practices and challenges for vision systems in industrial robotic grasping and assembly applications," *Advances in Industrial Engineering,* vol. 9, no. 1, pp. 19-30, 2020.

[2] R.Bogue, "Bin picking: a review of recent developments," *Industrial Robot* vol. 50, no. 6, pp. 873-877, 2023.

[3] Z.He, W.Feng, X.Zhao, and Y.Lv, "6D Pose Estimation of Objects: Recent Technologies and Challenges - Review," *Applied Sciences,* vol. 11, 2021.

[4] G.Marullo, L.Tanzi, P.Piazzolla, and E.Vezzetti, "6D object position estimation from 2D images: a literature review," *Multimedia Tools and Applications,* vol. 82, pp. 24605 - 24643, 2023.

[5] J. M. Fitzpatrick and J. B. West, "The Distribution of Target Registration Error in Rigid-Body Point-Based Registration," *IEEE Trans. Medical Imaging,* vol. 20, no. 9, pp. 917-927, 2001.

[6] M. H. Moghari and P. Abolmaesumi, "Distribution of Target Registration Error for Anisotropic and Inhomogeneous Fiducial Localization Error," *IEEE Trans. Medical Imaging,* vol. 28, no. 6, pp. 799-813, 2009.

[7] *Standard Test Method for Evaluating the Performance of Systems that Measure Static, Six Degrees of Freedom (6DOF), Pose*, ASTM E2919-13, 2013.

[8] H. Yang, J. Shi, and L. Carlone, "Teaser: Fast and certifiable point cloud registration," *IEEE Trans. on Robotics,* vol. 37, no. 2, pp. 314-333, 2021.

[9] P.Rachakonda *et al.*, "Towards the development of standards and performance metrics for 3D imaging systems " in *SPIE Defense + Commercial Sensing 2024*, National Harbor, MD, US, 2024: SPIE.

[10] T.Hodan *et al.*, "BOP Challenge 2020 on 6D Object Localization," *arXiv:2009.07378v2 [cs.CV],*

[11] R. Bregier, F. Devernay, L. Leyrit, and J. L. Crowley, "Symmetry Aware Evaluation of 3D Object Detection and Pose Estimation in Scenes of Many Parts in Bulk," presented at the ICCV, 2017.

[12] H.Zhao *et al.*, "Learning Symmetry-Aware Geometry Correspondences for 6D Object Pose Estimation," in *ICCV*, Paris, France, 2023, pp. 14045 - 14054.

[13] W.Niu, X.Huang, H.Xiang, X.Wang, and S.Ji, "A symmetry-aware alignment method for photogrammetric 3D models," *ISPRS Journal of Photogrammetry and Remote Sensing,* vol. 204, 2023.

[14] OpenCV. (2025). *Perception Challenge for Bin-picking*. Available: https://bpc.opencv.org

[15] A. Kirillov *et al.*, "Segment Anything," *arXiv:2304.02643v1 [cs.CV],*

[16] P. J. Besl and N. D. McKay, "A method for registration of 3-D shapes," *IEEE Trans. Pattern Analysis and Machine Intelligence,* vol. 14, pp. 239-256, 1992.

[17] M.Franaszek, P.Rachakonda, and K.S.Saidi, "Improving Fitting CAD to 3D Point Cloud Acquired with Line-of-Sight Sensor," presented at the IEEE Int. Symposium on Robotic and Sensors Environment ROSE'23, Tokyo, 2023.